REGULAR ARTICLE

The Influence of Glass Fiber and Copper Wire z-Binder on the Mechanical Properties of 3D Woven Polymeric Composites

A. Ashraf Ghandour[1] · A. I. Selmy[1] · M. Megahed[1] · A. M. Kabeel[1] · Ahmed Ibrahim[1]

Abstract

Three-dimensional composites (3D) have potential applications in various fields due to their enhanced properties compared to conventional two-dimensional composites (2D). This study investigates the effect of different volumes of z-binder made from copper wire and E-glass fiber on the mechanical properties of 3D woven polymeric composites. The tensile, flexural, and fracture toughness behavior of four types of 3D orthogonal woven composites were studied in addition to a comparative 2D composite. The creation of the 3D orthogonal single-ply fabrics involved weaving z-binders using two different copper wire diameters, single fiber bundles, and double fiber bundles, each combined with four layers of woven E-glass fiber. The consolidation process for both 2D fabric and single-fabric 3D woven composites was executed using the hand lay-up technique. The results showed that most 3D woven composites outperformed 2D composites in terms of fracture toughness (stress intensity factor K_{IC} and energy release rate G_{IC}) and flexural strain. However, a decrease in flexural strength and tensile properties was observed for all 3D composites. The specimen with a small copper diameter had the smallest decrease of 5% in tensile strength. Furthermore, a decrease of 9% and 21% was attained by reinforcing with double and single glass fiber bundle z-binders, respectively, as compared with 2D composites. The highest enhancement of 92.5% in flexural failure strain was attained with double glass fiber bundles of z-binder. The maximum improvement in K_{IC} fracture toughness, reaching 126% and 101.5%, was observed in specimens with a single glass fiber bundle z-binder and those with a large copper wire diameter, respectively.

Keywords Three-dimensional woven composites · Metal wire reinforcement · Fracture toughness · Orthogonal · Large flexural strain

1 Introduction

Composites offer substantial choice to the designer by permitting and optimizing the strength and stiffness of a structure for a specific application [1–7]. The utilization of three-dimensional woven composites is widespread in engineering and industry [8]. They are preferred in different applications, including spacecraft, different parts of aircraft such as fan blades and wing connectors, submarines, satellites, sporting goods, armored structures, civil infrastructure, wind turbine blades, pressure vessel stiffeners, rails, water vehicles, and automotive [9–16].

This is attributed to their advantages over conventional unidirectional (UD) and 2D composites, such as higher impact resistance and strength, superior delamination resistance, improved toughness, improved interlaminar tensile strength, the ability to be woven near net shape, a large production rate, low labor costs since there is no need for the ply lay-up process, and enhanced mechanical properties in the through-thickness direction [9, 10, 13, 15, 17–21]. In 3D woven composites, the fibers in the fabric are oriented in three directions (X, Y, and Z) in one single fabric, which reduces the occurrence of delamination because of the presence of fibers running through the thickness direction (z-binders) [22–24]. Three-dimensional woven composites can be categorized into three main architectural configurations: angle-interlock, layer-to-layer, and orthogonal [25]. Numerous studies have examined the 3D woven composites' mechanical performance, including tensile properties [16, 26–31], flexural

✉ A. Ashraf Ghandour
ahmedashraf.eng.zu@gmail.com

1   Department of Mechanical Design and Production Engineering, Faculty of Engineering, Zagazig University, P.O. Box 44519, Zagazig, Egypt

properties [29, 31–34], and fracture toughness [35–38]. However, limited research has compared these properties with those of 2D or UD composites. Generally, 3D woven composites demonstrate superior fracture toughness compared to their UD and 2D counterparts, although their in-plane properties such as flexural and tensile strength tend to be lower [10, 11, 22, 29, 39].

Examining the influence of fabric structure on tensile properties, Gu et al. [40] studied four glass/epoxy composites with structures of orthogonal, angle interlock, modified orthogonal, and modified angle interlock. The orthogonal structure exhibited superior properties due to its straight and less-crimped fibers. In addition, Warren et al. [9] studied 3D woven carbon/epoxy composites' mechanical tensile behavior, exploring the distinct responses exhibited by two architectural configurations: layer-to-layer and orthogonal, in addition to a comparative 2D composite under tensile and compressive loading. The orthogonal woven structure exhibited superior strength and modulus in tension and compression in the warp direction. Abbasi et al. [35] studied the fracture toughness behavior of 3D woven orthogonal composites, utilizing z-binders made from steel, copper, and carbon fiber with low and high z-binder volumes. In addition, a comparative 2D carbon fiber composite was produced. The study revealed that composites reinforced with z-binders exhibited significant improvements in fracture toughness. In addition, the tensile and flexural behavior of the same composite types were also investigated [11]. 2D composites had higher tensile and flexural properties, and increasing the volume of z-binder had no effect on those properties.

In a comparative investigation by Olhan et al. [29], the flexural and tensile behaviors of 3D orthogonal composites reinforced with either basalt or glass embedded in an epoxy matrix were compared to their 2D and UD counterparts. Notably, while UD and 2D composites excelled in tensile strength along both the warp and weft axes, 3D orthogonal composites demonstrated better flexural strength along the weft axis. Furthermore, Al-Nadhari A et al. [33] conducted a study exploring the influence of two distinct hybridization approaches utilizing polyethylene and Kevlar fibers in addition to glass fibers on the flexural behavior of 3D orthogonal composites, and flexural strains exceeding 10% were achieved.

Vishal et al. [41] studied the tensile behavior of four distinct hand-woven 3D orthogonal fabrics reinforced with carbon and Kevlar fibers, including two hybrid configurations. The binder was woven at 45 degrees to the weft and warp. The study revealed lower strength compared to their 2D woven counterparts. Korkmaz [32] reported that 3D woven orthogonal carbon fiber composites had lower flexural properties compared to 2D equivalents but had less delamination. Yang et al. [42] studied the bending properties of 3D carbon fiber/PEEK composites with varying resin content.

Their study revealed a superior bending strength compared to other thermoplastic carbon fiber composites reported in existing literature.

While conventional literature has predominantly utilized fibrous or polymer threads as z-binders (usually carbon or glass) due to their flexibility in the weaving process [35], thin metal wires have been scarcely explored. Sharp et al. [43] demonstrated the ability of copper wire to be orthogonally woven with carbon fiber fabrics, and Abbasi et al. [11, 35, 44–46] pioneered the study of metal z-filaments for enhancing properties like delamination resistance. Despite these advancements, the utilization of z-binders made from copper in 3D orthogonal woven E-glass/epoxy composites is unexplored. Limited literature has explored the role of z-binder volume in determining the mechanical performance of these materials [11]. Moreover, the application of the single edge notched beam (SENB) method in investigating fracture toughness is scarce, with most studies relying on end-notch flexure (ENF) or double cantilever beam (DCB). Additionally, existing literature has used advanced consolidation methods like infusion molding (RIM) and resin transfer molding (RTM), which elevate the overall manufacturing expenses.

This study is motivated by the aim of developing cost-effective polymeric 3D orthogonal woven composites. To achieve this objective, a comparative investigation was conducted on four distinct 3D orthogonal fabrics with different volumes of metal wire or glass fiber z-binder, using a simple manufacturing method without reducing in-plane fibers. Additionally, a comparative 2D woven composite was created. The mechanical properties of these newly developed composite materials were examined through a series of tests, including assessments of tensile properties, flexural behavior, and fracture toughness (utilizing the SENB method). To the best of the authors' knowledge, this study expands the horizons of 3D orthogonal woven polymeric composites by introducing glass fiber and copper wire z-binders with two different diameters in E-glass/epoxy through a cost-effective hand lay-up technique. Additionally, it provides the first reported stress intensity factor (K_{IC}) for fracture toughness in this context.

2 Experimental Work

2.1 Materials

Three distinct types of fiber reinforcements were employed in the fabrication of the 3D woven fabrics. These include unidirectional E-glass fiber roving, woven roving E-glass fiber, and copper wire. Specifically, the unidirectional fiber and copper wire serve as z-binders within the structure of the 3D woven composites. These constituents were selected

due to their widespread availability in the local market and cost-effectiveness. The woven roving E-glass fiber used is a plain weave with an equal thread count in both directions, weighing 600 g per square meter. The plain weave glass fiber and unidirectional E-glass were sourced from Hebei Yuniu Fiberglass Manufacturing Co. Ltd., China. Copper wire with two distinct diameters, namely 0.4 mm and 0.9 mm, was procured from Cooper Wiring, boasting a purity level of 99%. The selection of copper was predicated on its ductility [11], while fiberglass was chosen for its commonplace utilization in the local market. The epoxy resin utilized in this study is Kemapoxy 150 RGL.

2.2 Weaving of 3D Fiber Fabric Preforms

The 2D composite fabric is made of woven roving E-glass fiber and consists of four layers. The 3D woven composite had an orthogonal structure, as depicted in Fig. 1. The z-binders in these structures were fabricated using copper wire and E-glass fiber roving, each in two different diameters. The designations for the manufactured 2D and 3D composites, the calculated fiber volume fraction, and Z-binder volume content are detailed in Table 1. To minimize significant fabric deformation, the preferred diameter for the

Fig. 1 The 3D woven fabric's orthogonal architecture

copper wire was deliberately kept below 1 mm, in line with findings reported by Mouritz et al. [28].

All fabrics have four layers of dry E-glass fiber woven fabrics that were cut to equal dimensions. Each layer is then checked for alignment using a right-angle, and then all layers are pasted with tape at the edges. The same procedures were repeated for each layer; the layers were stacked together, making sure that warp tows were aligned in the same direction to create a cross-ply fiber pattern for the composite. The tape was used to make sure they were even, and no slippage occurred during the z-binder weaving process. For the 3D-woven fabrics, the z-binder in each fabric is manually woven using a sewing needle in an orthogonal direction. Figure 2 shows a sample of each 3D-woven fabric after weaving.

2.3 Composite Fabrication

The 2D and 3D composites were manufactured using the hand-layup technique. A composite material was fabricated by mixing epoxy 150 RGL and hardener in a 100:50 weight ratio. The fabric preform was subsequently impregnated with the epoxy mixture using a brush and roller, as indicated in Fig. 3. Curing the composite with a thick glass plate placed on top for 21 days at room temperature facilitated the elimination of excess epoxy.

2.4 Mechanical Testing

The evaluation of mechanical properties, encompassing tensile properties, flexural behavior, and fracture toughness, was conducted under standard room temperature conditions (23 °C) using a universal testing machine of the Jinan Test Machine WDW 100 KN type. Mechanical testing for each composite configuration employed three individual specimens, with reported values representing the calculated average. A computer system interfaced with the testing apparatus was employed to produce a record of load–displacement data.
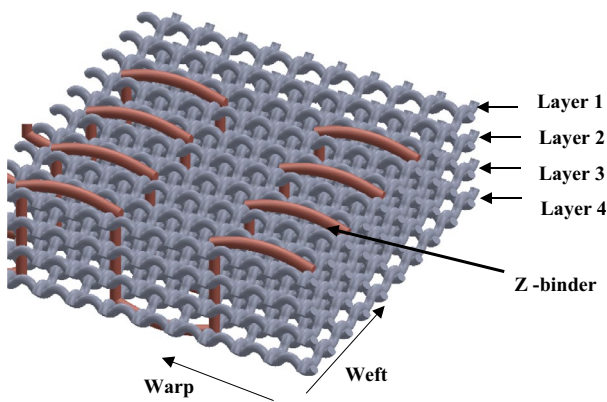
Table 1 3D woven composites' specifications

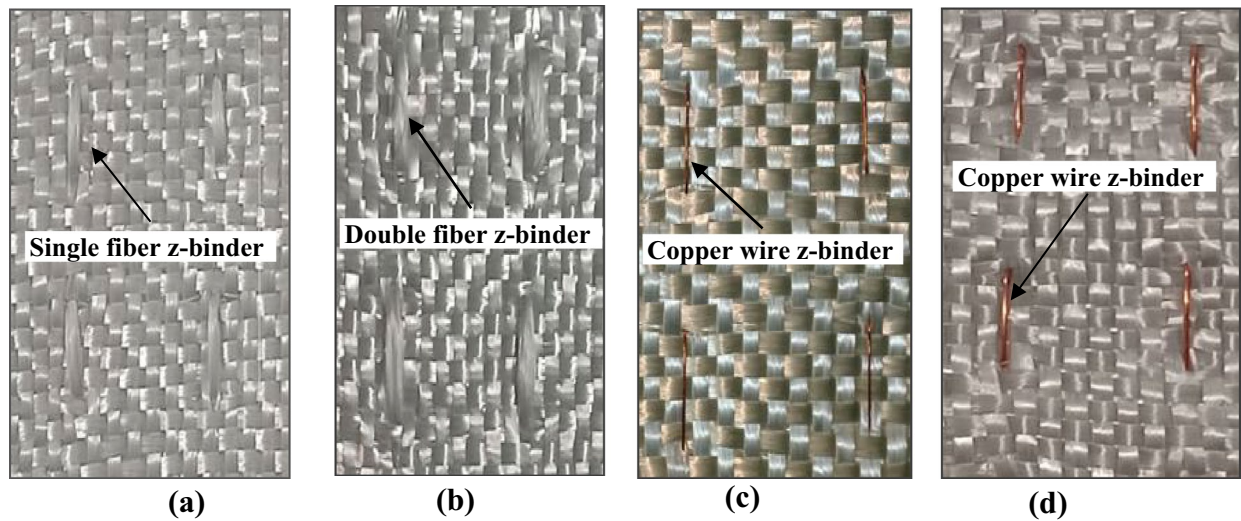| Specimen Code	Z-Binder Type	Z-Binder Specification	Structure	Fiber Volume Fraction %	Z-Binder Volume Content (%)
2WD	–	–	2 Dimension	39.67%	–
C1	Copper	Diameter = 0.4 mm	3D orthogonal woven	36.65%	0.32%
C2	Copper	Diameter = 0.92 mm	3D orthogonal woven	34.67%	1.53%
SF	E-glass roving	One bundle	3D orthogonal woven	38.54%	2.41%
DF	E-glass roving	Two bundles	3D orthogonal woven	39.56%	4.65%

Fig. 2 Different 3D woven fabric after weaving **a** SF, **b** DF, **c** C1, and **d** C2
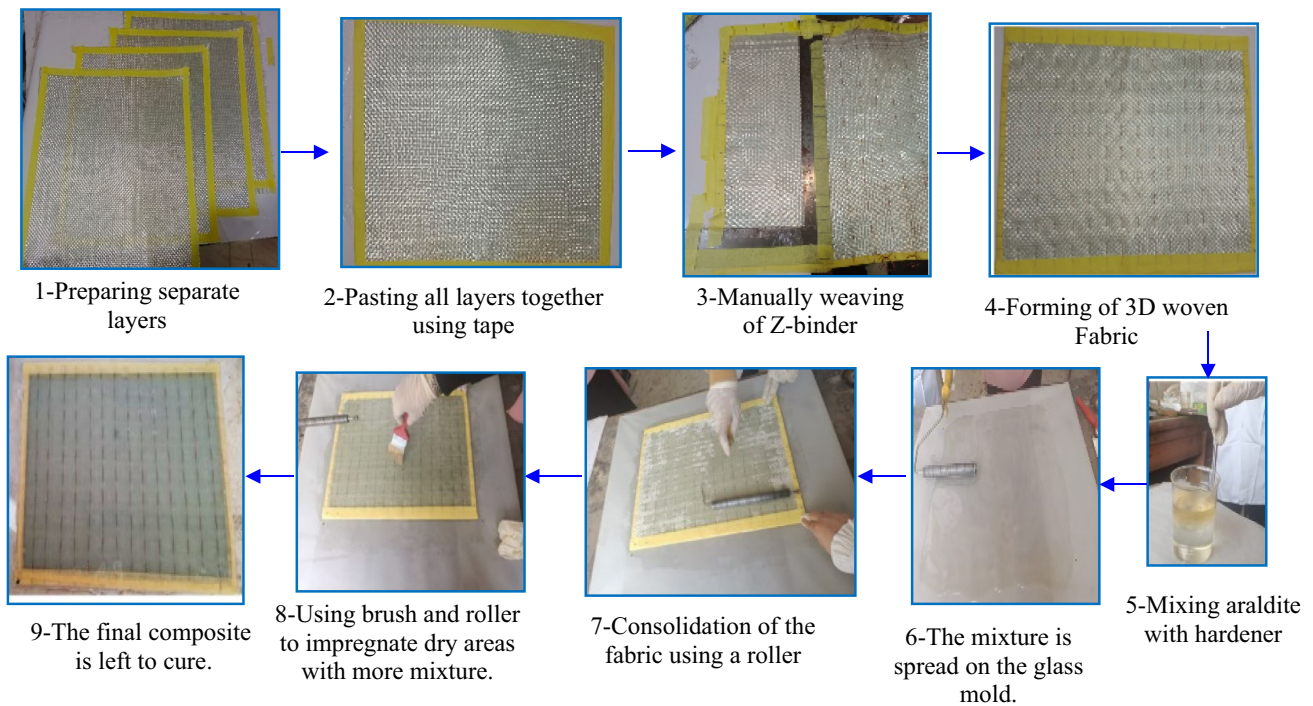

Fig. 3 Manufacturing steps of 3D composite

2.4.1 Tensile Test

The mechanical tensile behavior was evaluated for the fabricated composites in accordance with the specifications outlined in ASTM D3039. The speed of the cross head was maintained at 2 mm/min across all specimens during testing [47]. The specimens, prepared as strips with dimensions of 250 mm in length and 25 mm in width, were subjected to

tension testing. The universal testing machine provided the stress–strain curve, which served as the basis for calculating both the maximum tensile strength and the apparent tensile elastic modulus, as detailed below:

$$\sigma_{\text{ult}} = P_{\text{max}}/bh \tag{1}$$

$$E_{app} = \Delta\sigma_{ult} / \Delta\varepsilon_L \tag{2}$$

σ_{ult} denotes the peak stress observed on the stress–strain curve, signifying the material's maximum tensile strength; b and h denote specimen width and thickness, respectively; and P_{max} is the maximum tensile force. The apparent Young's modulus (E_{app}) is evaluated by measuring the slope of the elastic region (initial linear portion) of the stress–strain curve ($\Delta\sigma_{ult}/\Delta\varepsilon_L$).

2.4.2 Three-Point Flexural Test

In accordance with the specified guidelines of JISK7055, the three-point bending tests were carried out at a consistent crosshead speed of 2 mm/min to ensure uniform conditions. Specimens, measuring approximately 100 mm in length and 15 mm in width, were employed, maintaining a predetermined span-to-depth ratio of 16:1. Securely attached to the grips of the universal testing machine, the jig facilitated the bending test. The evaluation of flexural strength (σ_{fl}), flexural modulus (E_{fl}), and flexural strain (ε_{fl}) followed established relationships, as outlined below:

$$\sigma_{fl} = 3P_f L / 2bh^2 \tag{3}$$

$$E_{fl} = L^3 m / 4bh^3 \tag{4}$$

$$\varepsilon_{fl} = 6Dh / L^2 \tag{5}$$

In this context, P_f signifies the maximum flexural force, L denotes the distance between the supports (span length), m represents the slope of the initial straight portion of the load–deflection curve, and b and h denote the dimensional parameters of the specimen, representing its width and thickness, respectively.

2.4.3 Fracture Toughness Test

Fracture toughness is known as the material's resistance to crack propagation under applied stress. It's very important as it quantifies the stress amount required for pre-existing cracks to extend [48]. This work employed the single-edge notch bending (SENB) method, adhering to ASTM D5045 guidelines, to assess fracture toughness [6, 48, 49], but there is a scarcity of studies utilizing the SENB method to investigate the fracture toughness of 3D woven composites. To evaluate the fracture toughness of SENB specimens, a controlled three-point bending test was conducted at a precise displacement rate of 1 mm/min. Based on the measured data, both the critical strain energy release rate (G_{ic}) and the critical stress intensity factor (K_{IC}) were calculated based on the following formulation:

$$K_{IC} = \frac{P_I}{h\sqrt{w}} f(x) \tag{6}$$

$$f(x) = 6x^{0.5} \frac{[1.99 - x(1-x)(2.15 - 3.93x + 2.7x^2)]}{(1+2x)(1-x)^{3/2}} \tag{7}$$

$$G_{IC} = \frac{K_{IC}^2 (1 - v^2)}{E} \tag{8}$$

In this context, P_I represents the maximum load, x denotes the ratio of the length of the crack (a) to the specimen's width (w), h represents the specimen's thickness, and E is the tensile elastic modulus.

3 Results and Discussion

3.1 Tensile Test

Figure 4 depicts the tensile behavior of both 2D and 3D woven composites through their respective stress–strain curves. Notably, all types of 3D woven composites exhibit a decrease in tensile failure stress and strain compared to their 2D counterparts. This common behavior in 3D woven composites is primarily ascribed to the use of z-binder and its associated weaving process, which caused crimp, waviness, and weaving distortions such as broken fibers. Thus, the reduction in tensile properties may be due to the shear stress that results from the straightening of the z-binder and wavy plies near it in the tensile loading direction. The crimping process produces surface defects that serve as stress concentrators and lead to deeper matrix cracks, which decreases the mechanical properties of 3D composites. As a result, the crimping process has a significant impact on the failure mechanism of these materials [50]. The large area of
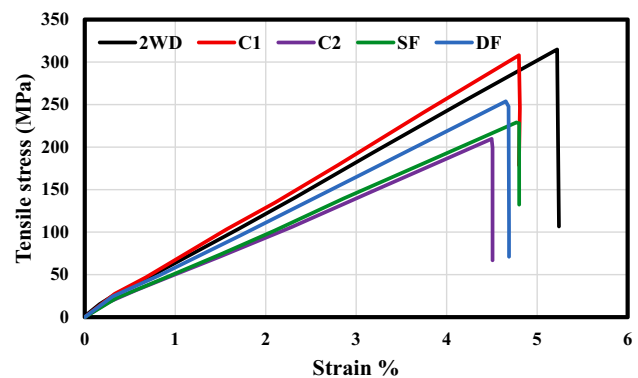

Fig. 4 Stress–strain curves for 2D and 3D woven composites under tensile loading

the z-binder also produced resin-rich. Previous research, as reported in [11, 26–31, 41], consistently observed a reduction in tensile behavior for 3D woven composites.

Figure 5a illustrates the average ultimate tensile strength values for 2D and 3D woven composites. Specimen C1 shows a slight decrease of 5% compared to 2D woven composites, exceeding the results reported by some studies [11, 29, 30]. A decrease of 21% and 9% was attained with SF and DF, respectively. In contrast, specimen C2 shows the largest decrease of 33% in ultimate tensile strength, surpassing values reported in other studies [29, 30]. The variance in results among copper specimens can be attributed to the diameter of copper, which exhibits lower tensile strength than fiberglass, leading to increased distortion in the woven structure.
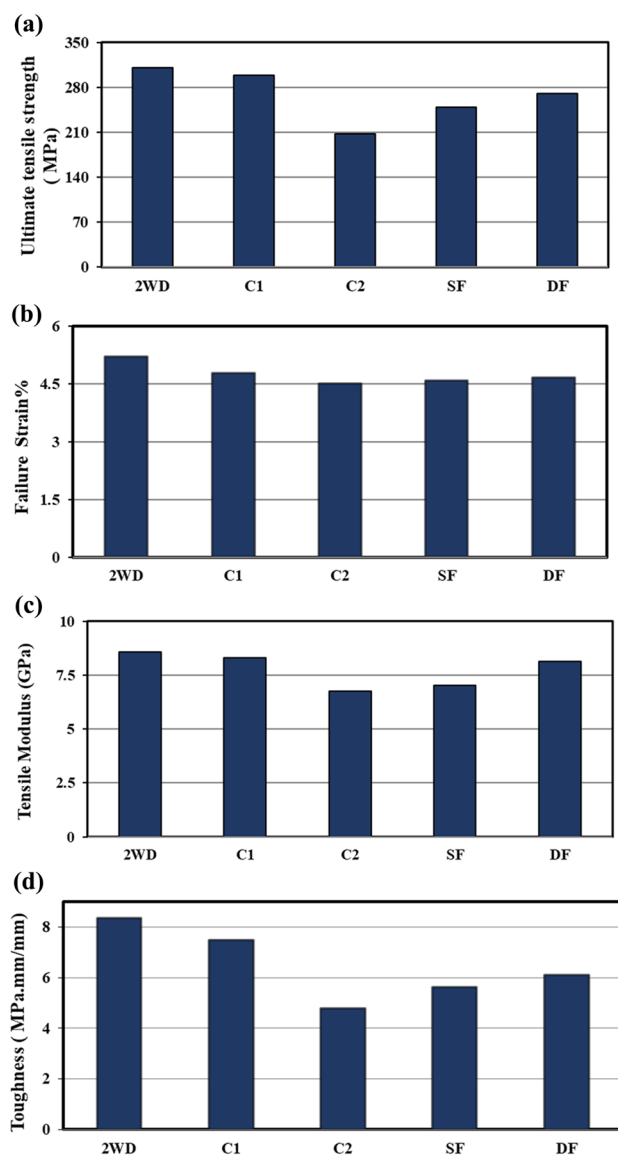

Fig. 5 2D and 3D woven composites' tensile properties: **a** ultimate tensile strength; **b** tensile strain; **c** tensile modulus; and **d** toughness

3D woven composites with glass fiber z-binder have values falling between C1 and C2, with double bundle specimens exhibiting larger strength than single bundle specimens due to more fibers in the loading direction. Single bundle fiber specimens show better ultimate tensile strength than C2.

The average failure strain values are presented in Fig. 5b. The 3D woven composites demonstrate a reduced strain at failure relative to the 2D specimens. This is consistent with findings by Abbasi et al. [11]. Tensile modulus values in Fig. 5c follow a similar trend to ultimate tensile strength, with 2WD, C1, and DF exhibiting closely aligned results. This reduction in tensile modulus is attributed to the distortion and crimp of the load-bearing yarns by the z-binders [51]. The elastic modulus was reduced due to inelastic tow straightening and cracking around the most heavily crimped in-plane tows. Extra softening occurred at higher strains by inelastic straightening of all the tows [13]. In addition to ultimate tensile strength and modulus, another important material property is toughness, defined as its capacity to absorb energy before breaking. This property can be directly assessed through the tensile test [52]. Figure 5d presents the measured toughness values, which exhibit a similar trend to the previously discussed mechanical properties.

In response to tensile loading, various damage mechanisms were observed in the tested composites, as indicated in Fig. 6, including matrix cracking and fiber breakage for both 2D and 3D woven composites subjected to tensile loading. Ultimate failure consists of the separation of the tensile coupon along a path comprising the first tension crack, the delamination crack, and a second tension crack traversing the rest of the specimen. Matrix cracking is usually found prior to any fiber rupture. Similar observations were reported by [31]. Notably, there was no evidence of delamination around the z-binder. This is indicated by the higher opaque region around failure in 2D composites, which is an obvious sign of internal damage. Similar observations were reported by Behera et al. [39] and Olhan et al. [29]. In all 3D specimens, minimal debonding was observed in the region around the z-binder, indicating the z-binder's ability to resist debonding between the layers. Also, it is noted that the z-binder copper wire type was almost dry, which means poor bonding between the copper reinforcement and the epoxy matrix was obtained.

3.2 Flexural Test

Figure 7 illustrates the flexural behavior through flexural stress–strain curves of the manufactured 2D and 3D woven composites. Interestingly, the last part of the curve for the 3D composites shows a noticeable non-linearity, whereas the 2D laminates show a sharp decline soon after total failure. The fiber bridging by z-binders, which act as a stitch bridging zone, is the cause of this nonlinearity.
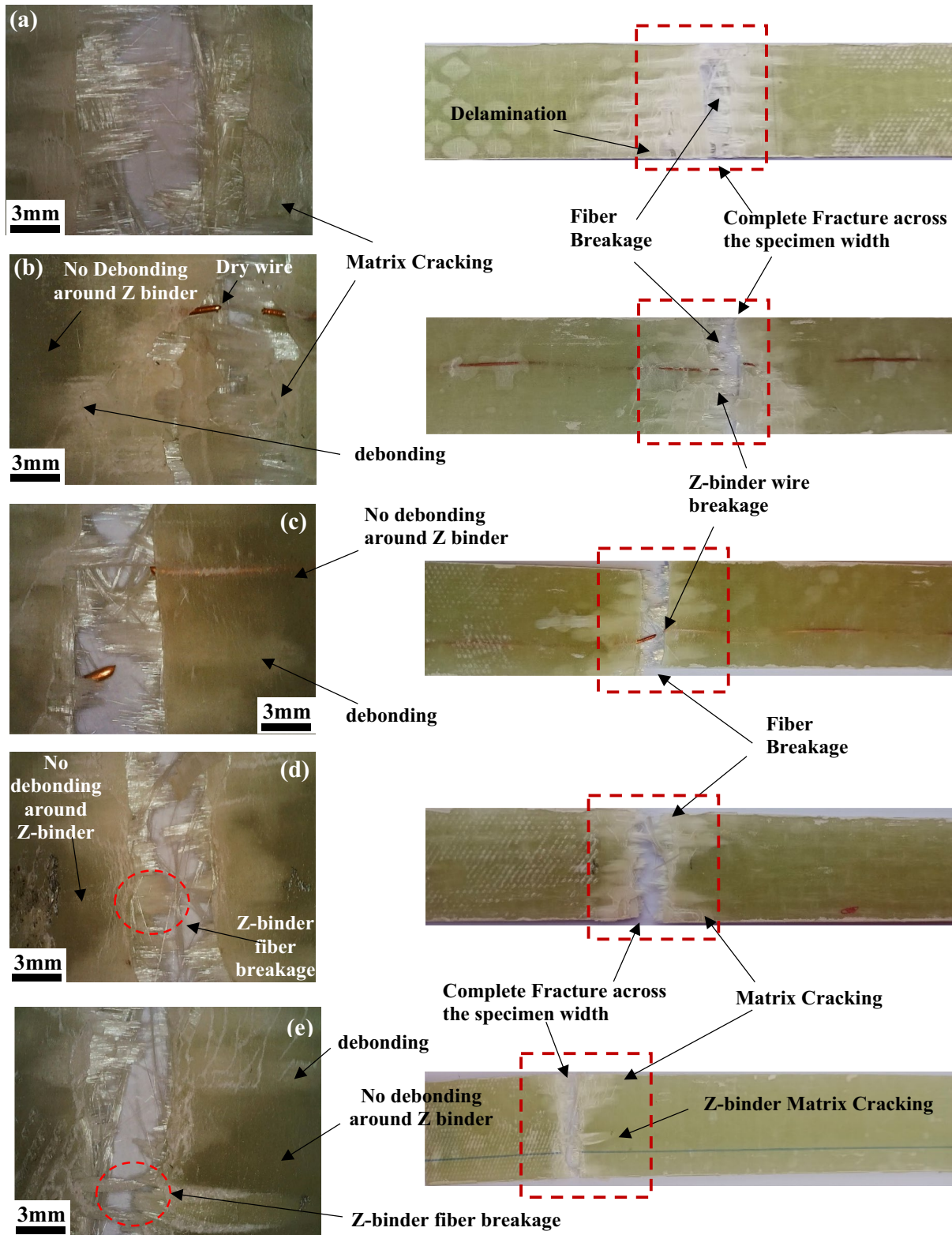
Fig. 6 2D and 3D woven composites' fractured specimens after tensile testing with microscopic view for **a** 2D, **b** C1, **c** C2, **d** SF, and **e** DF
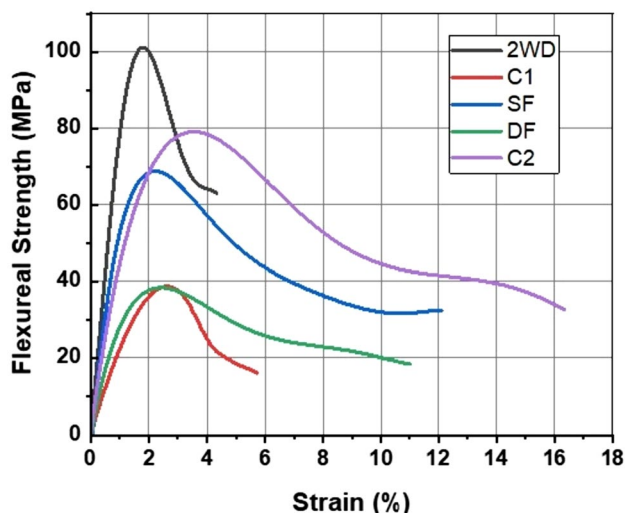
Fig. 7 2D and 3D woven composites' flexural stress–strain curve

Fig. 8 2D and 3D woven composites' flexural properties: **a** Flexural strength; **b** Flexural strain; and **c** Flexural modulus

First, there is delamination, which triggers the start of a stitch bridging phenomenon that initially slows down the delamination crack's growth. Second, when the bending load increases gradually, the delamination progresses and breaks the first reinforcing tow. It then moves on to the second tow, which encounters a similar situation. The cycle ends with total failure [50]. Figure 8a displays the average flexural strength of these specimens. It is noteworthy that 2WD exhibited higher flexural strength, as reported by other studies [11, 29, 31–34]. This may be attributed to the utilization of z-binders, which resulted in crimping of z-binders, fiber misalignment, and deformation of yarns in the loading direction. Fiber misalignment is considered a prevalent type of damage that can occur in 3D composite specimens. This defect emerges from the spreading of fibers within the plane due to the z-binder's weaving process, consequently inducing localized tension in the affected area. Moreover, the adhesion between the reinforcement and the surrounding matrix is negatively impacted by this misalignment, which reduces the mechanical performance of 3D composites, especially under bending loads [50].

On the other hand, all 3D woven composites demonstrated superior flexural strain. The use of z-binder, depending on its type, contributed to enhanced flexural strain compared to 2WD. This was considered a good result as compared with other studies [11, 26, 29, 31, 33].

In Fig. 8b, the average flexural strain at maximum load is illustrated. A remarkable enhancement of 92.5% in flexural strain was achieved with DF compared to 2WD. Additionally, flexural strain improved by 88.44%, 81.25%, and 50% with C1, C2, and SF, respectively, in comparison to 2WD. Conversely, Fig. 8c illustrates a decrease in flexural modulus for all 3D woven composites compared to 2WD.
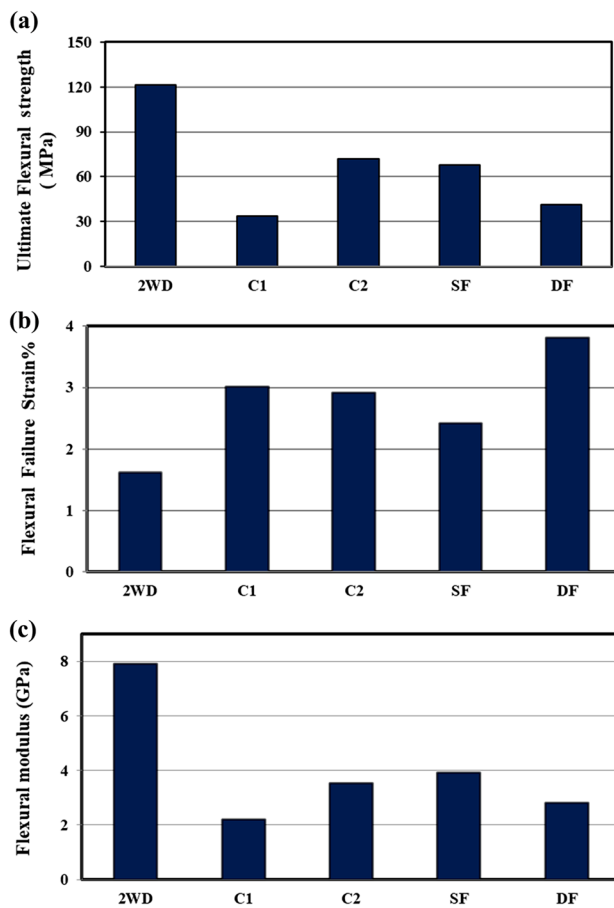
Similarly, Reis et al. [50] found that 3D composites displayed a 22% decrease in flexural strength and a 19% decrease in stiffness when compared to their 2D composite counterparts. This reduction was attributed to the damage incurred during the stitching process, including fiber breakage, misalignment, and the presence of resin-rich areas. Fiber rupture around stitching points failed to support compressive stresses on the upper portion of the composites, thereby overloading nearby fibers. Additionally, the development of kinking bands on the composite's surface is prone to occur in areas of significant misalignment and crimping. The combined effects of these mechanisms lead to early failures in 3D composites, which in turn result in decreased flexural elastic modulus and strength.

Despite the ability of the C2 specimen to undergo a high failure strain of up to 16%, attributed to the ductility of copper, the highest strain at maximum load was obtained for the DF specimen. Figure 9 visually represents the damage mechanism observed during flexural loading, and the opaque area demonstrates failure. Failures occurred in the mid-span of all specimens at the compression and tension sides. The
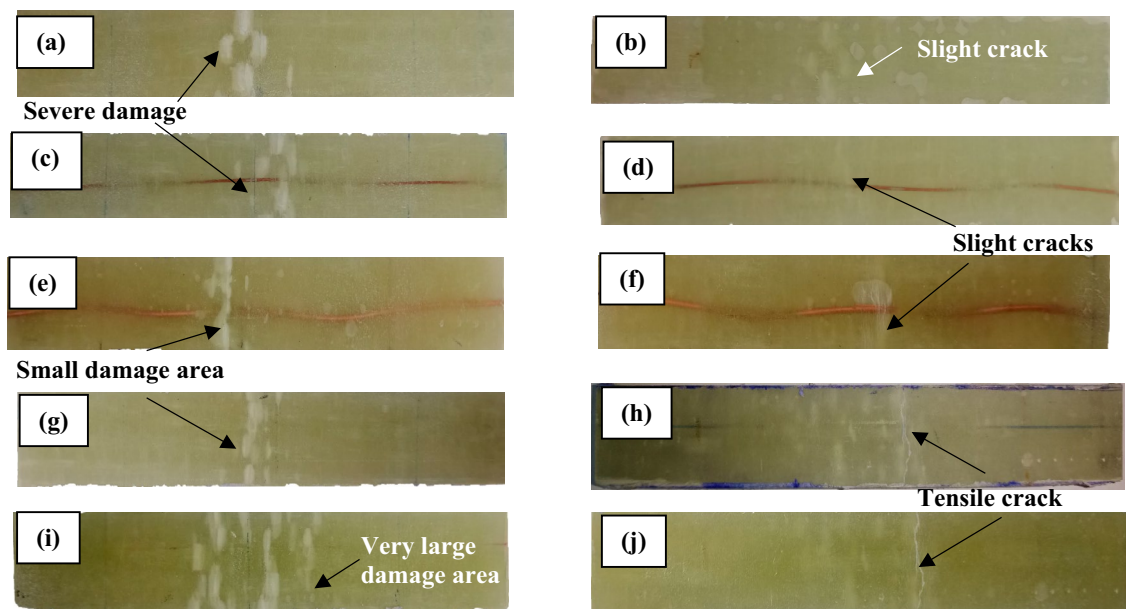
Fig. 9 Fracture surface for 2D and 3D composites' specimens following exposure to a three-point bending test for compression side **a** 2WD, **c** C1, **e** C2, **g** SF, and **i** DF, and for tension side **b** 2WD, **d** C1, **f** C2, **h** SF, and **j** DF

failure behavior aligns with the findings reported in references [39] and [53]. The innermost layer experiences compressive forces, resulting in kink-band failure. In addition, cracks are formed on the tension side, where the material undergoes tensile forces, primarily affecting the outermost layer.

Notably, all specimens, excluding C2, exhibited a high ability to recover their original shape after loading (shape recovery effect), which is particularly advantageous for repair applications. SF and DF specimens demonstrated a nearly complete return to their original shape. This happened without using any other alloys or other constituents.

3.3 Fracture Toughness Test

A notable improvement in fracture toughness is one of the main benefits that 3D composites are expected to bring about. The Z-binder reinforcement has been shown to be highly effective in suppressing the propagation of delamination cracks in comparison to 2D and 3D composites [35, 54, 55].

Although the strain energy release rate G_{IC} is a good measure to assess fracture toughness, the stress intensity factor K_{IC} is more practical in engineering applications. It specifies the critical stress level at which cracks will rapidly propagate and offers insights into the strains and stresses surrounding the tip of the crack. [56]. Therefore, it is widely used, and this is the first time that K_{IC} has been reported for 3D orthogonal fiber reinforced polymeric composites, while most papers focus on G_{IC} values only.

Figure 10a presents the fracture toughness critical stress intensity factor (K_{IC}) values. Notably, when compared to 2D specimens, SF specimens exhibited the maximum improvement in fracture toughness, with an impressive enhancement of 126.2%. Additionally, C2 and DF specimens demonstrated enhancements of 101.5% and 76%, respectively. The fiber bridging mechanism by z-binders in 3D composites
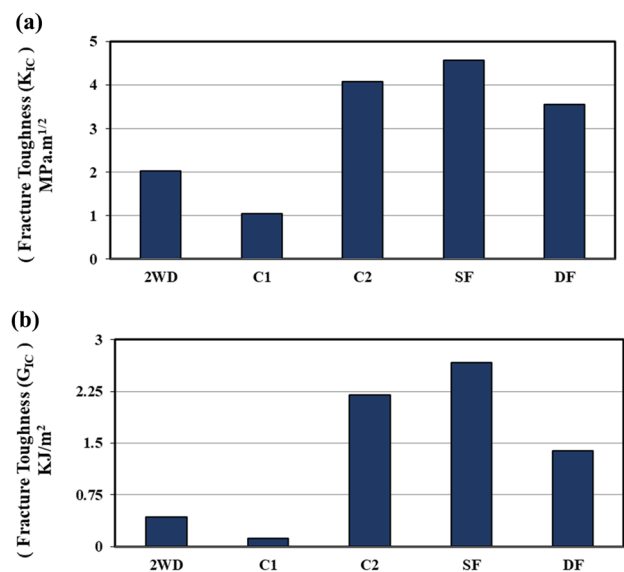

Fig. 10 Fracture toughness of 2D and 3D woven composites: **a** K_{IC} and **b** G_{IC} values

efficiently hinders delamination crack propagation, which is a critical failure mode in composites.

G_{IC} (which is the critical energy release rate) is illustrated in Fig. 10b, and it shows a similar pattern to K_{IC}. Significant improvement is observed in SF specimens, with an enhancement of approximately 520% in comparison to 2D specimens. This is followed by C2 and DF specimens, exhibiting improvements of 410% and 220%, respectively. The SF specimens outperform those of Abbasi et al. [35], which recorded a G_{IC} value of approximately 2.4 kJ/m^2 for 3D orthogonal carbon fiber/epoxy with a copper z-binder and 32 carbon fiber plies, by around 10%. Nevertheless, the C2 specimens exhibit a slight performance decrease of about 8% in comparison to Abbasi et al.'s [35] results. Other studies on 3D woven composites with an orthogonal structure [36–38] report similar G_{IC} values for DF, C2, and SF.

This significant improvement in both G_{IC} and K_{IC} can be attributed to the z-binder's role in retarding crack propagation, as evident in Fig. 11c, d, and e. There was not a noticeable amount of fiber breaking near the z-binder fiber. The manual weaving approach may be credited with mitigating this specific problem. It is noteworthy that the use of automated machines in stitching or weaving often leads to significant fiber misalignment, abrasion, breakage, and crimping within the plane [50, 51].

Nevertheless, a reduction in fracture toughness was evident in specimen C1 as compared to the 2WD counterpart. This decline is attributed to the smaller diameter of the copper z-binder, which lacks the necessary resistance to impede crack propagation, as illustrated in Fig. 11a, b. The K_{IC} values dropped by approximately 48%, and the G_{IC} values experienced a decline of around 72%.

4 Conclusions

The fabrication of 3D woven orthogonal composites utilizing metal and glass fiber z-binders with varying diameters was successfully achieved through a cost-effective and simple hand lay-up technique. Subsequently, 3D woven composites' mechanical behavior was investigated against a 2D conventional woven glass fiber/epoxy composite produced using the same method. The observed decrease in tensile strength in 3D composites woven with the smallest diameter of copper wire was minimal compared to findings in other studies. Additionally, all 3D woven composites exhibited high flexural strain in comparison to their 2D counterparts. However, the 3D composites demonstrated lower flexural and tensile strength compared to their 2D counterparts, consistent with existing research. This is attributed to distortions and crimp affecting the mechanical behavior under in-plane loading, in addition to the bonding quality between the copper reinforcement and epoxy matrix. Bending specimens (except C1) showed a great ability to restore their original shape even after undergoing significant deformations, particularly those with glass fiber z-binders. These insights are valuable for applications in which flexural properties and shape recovery are critical considerations. Moreover, the fracture toughness stress intensity K_{IC} factor has been reported for the first time for 3D woven orthogonal composites. Most 3D woven composite specimens showed a significant improvement in fracture toughness, reaching around 126% in K_{IC}, and a maximum G_{IC} was attained with single-bundle glass fiber z-binders. These enhancements outperform values reported in other composites made with more expensive methods using carbon and glass fibers. This highlights the effectiveness of the Z-binder in slowing down crack growth and suggests the potential for the use of this simple and cost-effective manufacturing technique on a large scale. Utilizing the hand weaving method is low-cost but requires skill and results in more weave damage. Generally, this study demonstrates that the developed 3D woven composites offer a cost-effective alternative for a range of structural applications, especially those demanding improved flexural strain and fracture toughness, such as vehicles, aircraft, and building structures.
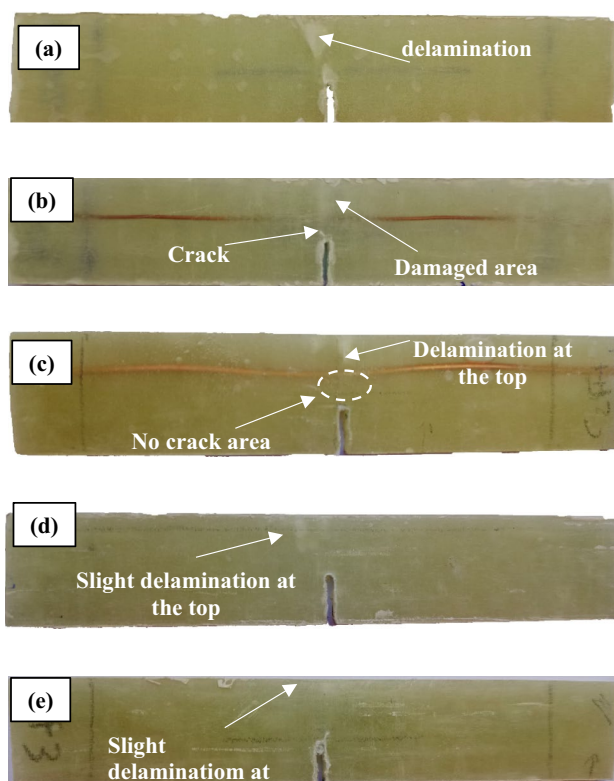

Fig. 11 Failure of specimens of 2D and 3D woven composites after fracture toughness testing: **a** 2WD, **b** C1, **c** C2, **d** SF, and **e** DF

Data Availability The datasets used during the current study are available from the corresponding author on reasonable request.

Declarations

Conflict of Interest The authors declare no conflict of interest.

References

1. M.A. Abd El-Baky, M.A. Attia, J. Thermoplast. Compos. Mater. Thermoplast. Compos. Mater. **32**, 228 (2019)
2. M.A. Abd El-Baky, M.A. Attia, J. Nat. Fibers. **18**, 213 (2021)
3. M.E. Naguib, S.I. Gad, M. Megahed, M.A. Agwa, Eng. Fract. Mech.Fract. Mech. **295**, 109751 (2024)
4. M. Megahed, S.M. Youssef, S.S. Ali-Eldin, M.A. Agwa, Fibers Polym. **22**, 1063 (2021)
5. M. Agwa, S.M. Youssef, S.S. Ali-Eldin, M. Megahed, J. Ind. Text. **51**, 5113S (2022)
6. M. Megahed, M. Agwa, A. Megahed, J. Ind. Text. **51**, 2944S (2022)
7. A. Megahed, M. Agwa, M. Megahed, J. Ind. Text. **51**, 1118S (2022)
8. X. Wang, T. Zheng, Z. Li, L. Guo, Compos. Sci. Technol. **245**, 110317 (2024)
9. K.C. Warren, R.A. Lopez-Anido, J. Goering, Compos. Part A Appl. Sci. Manuf. **73**, 242 (2015)
10. V. Goud, D. Singh, A. Ramasamy, A. Das, D. Kalyanasundaram, Compos. Part A Appl. Sci. Manuf. **130**, 105733 (2020)
11. S. Abbasi, Three-Dimensional Multifunctional Woven Composites Containing Through-Thickness Metal Filaments, RMIT University; Doctor of Philosophy (PhD), 2020. https://researchrepository.rmit.edu.au/esploro/outputs/9921898709101341.
12. M.N. Saleh, A. Yudhanto, P. Potluri, G. Lubineau, C. Soutis, Compos. Part A Appl. Sci. Manuf. **90**, 577 (2016)
13. P.J. Callus, A.P. Mouritz, M.K. Bannister, K.H. Leong, Compos. Part A Appl. Sci. Manuf. **30**, 1277 (1999)
14. Q. Hu, H. Memon, Y. Qiu, W. Liu, Y. Wei, Materials (Basel) **13**, 1 (2020)
15. M.H. Peerzada, S.A. Abbasi, A. Khatri, Sci. Int. **24**, 47 (2012)
16. M. Rubino, A. Mendoza, Y. Wielhorski, K.K. Parvathaneni, S. Roux, Comput. Methods Appl. Mech. Eng.. Methods Appl. Mech. Eng. **418**, 116559 (2024)
17. A.E. Bogdanovich, Multi-scale modeling, stress and failure analyses of 3-D woven composites. J. Mater. Sci. **41**, 6547–6590 (2006)
18. S. Ahmed, X. Zheng, L. Yan, C. Zhang, X. Wang, Compos. Sci. Technol. **199**, 108326 (2020)
19. L. Turpin, J. Neggers, A. Mendoza, J. Schneider, Y. Pannier, S. Roux, Eur. J. Mech. A/Solids **103**, 105166 (2024)
20. Z.P. Wang, B.N. Cox, S.J. Kuehsamy, M.H. Jhon, O. Sudre, N. Sridhar, G.J. Conduit, CAD Comput. Aided Des. **167**, 103637 (2024)
21. M.A. Abd El-baky, D.A. Hegazy, M.A. Hassan, M. Kamel, J. Compos. Mater. **56**, 1901 (2022)
22. P. Turner, T. Liu, X. Zeng, Compos. Struct.Struct. **142**, 286 (2016)
23. A.E. Bogdanovich, ICCM Int. Conf. Compos. Mater. (2007).
24. M. Dahale, G. Neale, R. Lupicini, L. Cascone, C. McGarrigle, J. Kelly, E. Archer, E. Harkin-Jones, A. McIlhagger, Compos. Struct.Struct. **223**, 110947 (2019)
25. M.N. Saleh, C. Soutis, Mech. Adv. Mater. Mod. Process. 3, (2017).
26. S. Dai, P.R. Cunningham, S. Marshall, C. Silva, Compos. Part A Appl. Sci. Manuf. **69**, 195 (2015)
27. P. Tan, L. Tong, G.P. Steven, T. Ishikawa, Compos. Part A Appl. Sci. Manuf. **31**, 259 (2000)
28. A.P. Mouritz, B.N. Cox, Compos. Part A Appl. Sci. Manuf. **41**, 709 (2010)
29. S. Olhan, B.K. Behera, J. Manuf. Process. **102**, 608 (2023)
30. J. Brandt, K. Drechsler, F.J. Arendts, Compos. Sci. Technol. **56**, 381 (1996)
31. B.N. Cox, M.S. Dadkhah, W.L. Morris, J.G. Flintoff, Acta Metall. Mater. Metall. Mater. **42**, 3967 (1994)
32. M. Korkmaz, Polym. Compos. 1 (2023).
33. A. Al-nadhari, H. Senol, S. Topal, H. Ulus, M. Yildiz, Compos. Part A **175**, 107753 (2023)
34. T. Huang, Y. Wang, G. Wang, Polym. Plast. Technol. Eng.. Plast. Technol. Eng. **57**, 740 (2018)
35. S. Abbasi, R.B. Ladani, C.H. Wang, A.P. Mouritz, Compos. Sci. Technol. **198**, 108301 (2020)
36. A.P. Mouritz, C. Baini, I. Herszberg, Compos. Part A Appl. Sci. Manuf. **30**, 859 (1999)
37. V.A. Guénon, T.W. Chou, J.W. Gillespie, J. Mater. Sci. **24**, 4168 (1989)
38. D.T. Fishpool, A. Rezai, D. Baker, S.L. Ogin, P.A. Smith, Plast. Rubber Compos. **42**, 108 (2013)
39. B.K. Behera, B.P. Dash, Mater. Des. **67**, 261 (2015)
40. H. Gu, Z. Zhili, Mater. Des. **23**, 671 (2002)
41. R.V. G, D. Singh, S.H. V, Int. J. Integr. Eng. **15**, 167 (2023)
42. X. Yang, L. Zheng, H. Ma, Z. Lu, F. Xu, Compos. Struct.Struct. **324**, 117559 (2023)
43. K. Sharp, A.E. Bogdanovich, W. Tang, D. Heider, S. Advani, M. Glowiana, AIAA J. **46**, 2944 (2008)
44. S. Abbasi, R.B. Ladani, C.H. Wang, A.P. Mouritz, Mater. Des. **195**, 109014 (2020)
45. S. Abbasi, R.B. Ladani, C.H. Wang, A.P. Mouritz, Compos. Part A Appl. Sci. Manuf. **147**, 106440 (2021)
46. S. Abbasi, R.B. Ladani, C.H. Wang, A.P. Mouritz, Compos. Struct.Struct. **260**, 113509 (2021)
47. H. Alshahrani, T.A. Sebaey, D.A. Hegazy, M.A.A. El-baky, Polym. Adv. Technol.. Adv. Technol. **33**, 2921 (2022)
48. M. Megahed, M.A. Abd El-baky, A.M. Alsaeedy, A.E. Alshorbagy, Fibers Polym. **22**, 1366 (2021)
49. A.A. Megahed, F. Abd El-Wadoud, A. Wagih, A.M. Kabeel, Compos. Struct.Struct. **263**, 113695 (2021)
50. L.M.M. Reis, M.L. Ribeiro, F. Madureira, A.C. Morelli, S.N. Monteiro, V.L. Arantes, J. Mater. Res. Technol. **29**, 90 (2024)
51. L. Lee, S. Rudov-Clark, A.P. Mouritz, M.K. Bannister, I. Herszberg, Compos. Struct.Struct. **57**, 405 (2002)
52. H. Khoramishad, H. Alikhani, S. Dariushi, Compos. Struct.Struct. **201**, 561 (2018)
53. Y. Liu, C. Huang, H. Xia, Q.Q. Ni, Mater. Des. **212**, 110267 (2021)

54. C. Hui, C. Chen, X. Legrand, P. Wang, Polymers (Basel) **14**, 1 (2022)

55. M.D.K. Wood, X. Sun, L. Tong, A. Katzos, A.R. Rispler, Y.W. Mai, Compos. Sci. Technol. **67**, 1058 (2007)

56. T.L. Anderson, *Fracture Mechanics* (CRC Press, 2017)